One-Step Integration of Sulfonated Polymer Films with Separators for Shuttle Mitigation in Lithium-Sulfur Batteries

Louisa C. Greenburg[#1], Kristen Abels[#2], Yukio Cho[2,6], Huayue Ai[3], Yi Cui[1,4,5*], William Tarpeh[2*], Yan-Kai Tzeng[6,*]

[1]Department of Materials Science and Engineering, Stanford University, Stanford, CA 94305, USA.

[2]Department of Chemical Engineering, Stanford University, Stanford, CA 94305, USA

[3]Department of Chemistry, Stanford University, Stanford, CA 94305, USA

[4]Stanford Institute for Materials and Energy Sciences, SLAC National Accelerator Laboratory, 2575 Sand Hill Road, Menlo Park, CA 94025, USA.

[5]Department of Energy Science and Engineering, Stanford University, Stanford, CA 94305, USA.

[6]SLAC-Stanford Battery Center, SLAC National Accelerator Laboratory, Menlo Park, CA, USA.

[#]These authors contributed equally.

[*]Correspondence to:

E-mail address: wtarpeh@stanford.edu (W.A. Tarpeh), yicui@stanford.edu (Y. Cui), ytzeng@slac.stanford.edu (Y.-K. Tzeng)

Abstract

Interfacial polymerization (IP) offers a rapid and inexpensive method to fabricate thin polymer films. In this work, a one-step, scalable IP reaction between a tri-acyl chloride monomer and sulfonated diamine monomer is employed to add a dense, charge-selective sulfonated thin-film coating onto a commercial separator to improve selective transport in lithium-sulfur batteries. The coating effectively suppresses polysulfide shuttling, enhancing capacity retention, though at the expense of compromised rate performance due to hindered lithium conduction through the dense film. Fractional substitution of the tri-functionalized acyl chloride monomer for a di-functionalized analog reduces the film crosslink density, which improves rate performance but decreases uniformity in film coverage. Uniform film coverage is achieved upon addition of a small fraction (0.25 wt%) of higher reactivity, non-sulfonated diamine in the IP reaction. This optimized thin film coating breaks the rate-capacity retention tradeoff, enabling a capacity of 885.5 mAh g^{-1} after 100 cycles at 0.2 C while still reaching over 800 mAh g^{-1} during rate testing at 2 C.

1 Introduction

The lithium-sulfur (Li-S) battery is an encouraging chemistry to increase the energy density over the state-of-the-art lithium-ion battery (LIB). Current battery electric vehicles typically use LIBs with an energy density up to around 250 Wh kg^{-1}, while Li-S batteries could achieve a practical energy density over 500 Wh kg^{-1}. [1,2] Further, unlike many typical LIB cathode materials, sulfur is environmentally friendly, abundant, and low-cost.[3] Despite its advantages, the sulfur cathode presents several obstacles that have delayed its commercialization. Notably, sulfur undergoes a conversion reaction through many intermediate lithium polysulfide phases before reduction to the final discharge product, lithium sulfide.[4] Most of these intermediates are soluble in the conventional ether electrolyte used in Li-S batteries. These soluble sulfur active materials can diffuse through the separator, causing capacity fade and self-discharge. As a result, Li-S batteries often suffer from poor cycle and calendar life.[4] Furthermore, the reduction of these species on the anode leads to higher impedance and poor lithium plating/stripping behavior.[5]

To address the challenges posed by the shuttle effect, a wide range of mitigation strategies have been investigated. Considerable effort has gone towards cathode engineering. Due to the insulating nature of sulfur, carbon additives or hosts should be added to the cathode, and a variety has also been shown to inhibit the polysulfide shuttle.[6] Other cathode strategies include designing coatings around sulfur or lithium sulfide particles to confine the active material (physically and/or via favorable adsorption),[7] adding catalysts to adsorb polysulfides while accelerating their conversion,[8] and engineering other unique sulfur nanostructures.[9–11] In addition, various electrolyte engineering efforts have shown that additives such as lithium nitrate can significantly decrease the capacity decay from active material loss.[12–14]

Beyond electrode and electrolyte engineering efforts, one facile and low-cost strategy to mitigate shuttle effects is polymeric separator modification.[15] The most common polypropylene (PP), polyethene (PE), or composite (PP/PE/PP) commercial battery separators electrically isolate the cathode and anode, but their high porosity and large pore size (on the order of tens of nanometers)[16] do not offer a sufficient barrier to polysulfide shuttling. Cathode-side separator coating with polysulfide-rejecting or stabilizing films has therefore been investigated for shuttle effect mitigation. These research efforts include separator modification with carbon materials[17,18], inorganic thin films,[19] metal organic frameworks (MOFs),[20] covalent organic frameworks (COFs),[21] and polymeric thin films (e.g. zwitterionic films,[22] negatively charged cation exchange films,[23,24] or combinations thereof[25]). Recent reviews summarize the efficacy of such modification strategies, which aim to enhance cycling performance (via polysulfide shuttling mitigation and/or mediation of LiPS reconversion) without impeding lithium ion conduction to simultaneously maintain desirable capacity and rate performance.[26,27]

Of all the aforementioned separator modification strategies, interfacial polymerization (IP) of a thin film polymeric coating directly on the conventional separator offers the benefits of scalability and low-cost preparation.[28] Traditional interfacial polymerization of diamine and acyl chloride monomers – such as m-phenylenediamine (MPD) or piperazine (PIP) with trimesoyl chloride (TMC) – is widely used for roll-to-roll reverse osmosis and nanofiltration polyamide thin film composite membrane fabrication.[29] The dense thin film active layer produced from interfacial polymerization offers excellent size-based solute rejection in traditional water treatment applications. Recent work has expanded interfacial polymerization chemistries to sulfonate containing groups to create a new class of thin film composite cation exchange membranes.[30] The fixed negative charge present in such membranes adds the additional charge-based selectivity mechanism for solute transport, enabling high cation conduction and anion rejection in electrochemical systems. In the application of Li-S separator modification, a thin film cation exchange membrane fabricated via interfacial polymerization could offer both size- and charge-based polysulfide rejection mechanisms, with more rapid and lower cost fabrication compared to perfluorinated cation exchange membrane counterparts (e.g., Nafion).

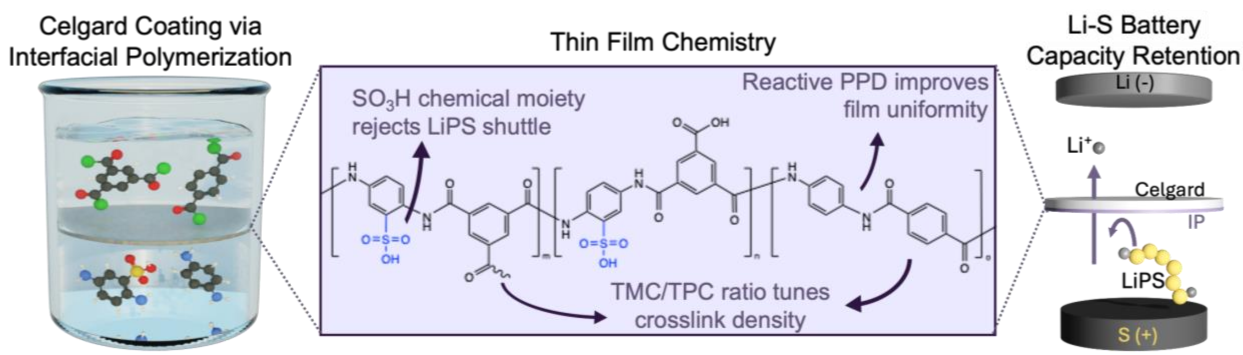

Figure 1: Schematic diagram of interfacial polymerization process on the Celgard separator. The thin film chemistry is designed to uniformly reject lithium polysulfide diffusion while allowing Li+ transport to enhance lithium-sulfur battery cycle life.

In this work, a rapid and facile interfacial polymerization method is investigated for surface modification of the Celgard tri-layer PP/PE/PP separator using a thin-film cation exchange membrane, depicted schematically in **Figure 1**. One-step interfacial polymerization of a sulfonated polyamide network is first demonstrated, formed by reacting TMC and 2,5-diaminobenzene sulfonic acid (DABSA). Reaction of the tri-acyl chloride-functionalized TMC with the diamino-functionalized DABSA enables the formation of a dense, crosslinked polymer network. To examine the influence of crosslink density on cell performance, a fraction of TMC is gradually substituted with the di-functionalized terephthaloyl chloride (TCL) monomer to produce films with reduced crosslinking. The effect of incorporating small amounts of p-phenylenediamine (PPD), the non-sulfonated analog of DABSA, is also evaluated to improve film formation and uniformity.

This systematic study reveals a trade-off between maintaining rate performance and capacity retention: less dense, low TMC films are required for sufficient sulfur kinetics, but denser films are required for mitigating polysulfide shuttle. A film made from 20% TMC-80% TCL in the organic phase is able to facilitate good sulfur kinetics to 2 C, yet fails to maintain the uniformly dense film required for long-term capacity retention. To overcome this trade-off, we find that adding a small fraction of higher-reactivity PPD to the DABSA solution yields a 20%TMC-80%TCL film that maintains good rate performance, while H-cell experiments demonstrate superior shuttle mitigation over the DABSA films without PPD. Overall, this study highlights the potential of this low-cost, one-step interfacial polymerization approach for separator modification in Li-S batteries and provides practical guidance for further optimization of coating strategies.

2 Results and Discussion

2.1 Probing Interfacial Polymerization of a Sulfonated Thin Film on Celgard

The monomers chosen for exploration, TMC and TCL in hexane and DABSA and PPD in water, are depicted in **Figure 2a**. Triethylamine (TEA) is added to the aqueous phase and serves as a proton scavenger that accelerates the polymerization reaction. TMC, with three acyl chloride groups, and TCL, with two acyl chloride groups, were chosen for the organic phase monomers to explore the effect of film crosslink density on capacity retention and rate performance. DABSA was selected as the aqueous phase sulfonated diamine to generate a thin film cation exchange membrane with negative fixed charge. PPD was added as a secondary, more-reactive diamine to enhance film formation. The polyamide thin film was formed directly on the commercial Celgard 2325 (PP/PE/PP, 25 μm) separator. In a glass scintillation vial, a 3 cm^2 circular Celgard separator is placed on the aqueous phase surface, followed by the organic phase solution (**Figure 2b**). Typically, the organic phase reagents migrate through the Celgard and polymerization begins at the Celgard/aqueous phase interface. The reactions were allowed to proceed for two hours at room temperature. The resulting membrane adheres to the Celgard which remains at the interface over the course of the reaction (**Figure 2c**). Through a temporal study on DABSA/TMC interfacial polymerization, we found that two hours allowed for sufficient time for DABSA to react and most significantly enhance the capacity of the sulfur cathode (**Supplementary Figure 1**).

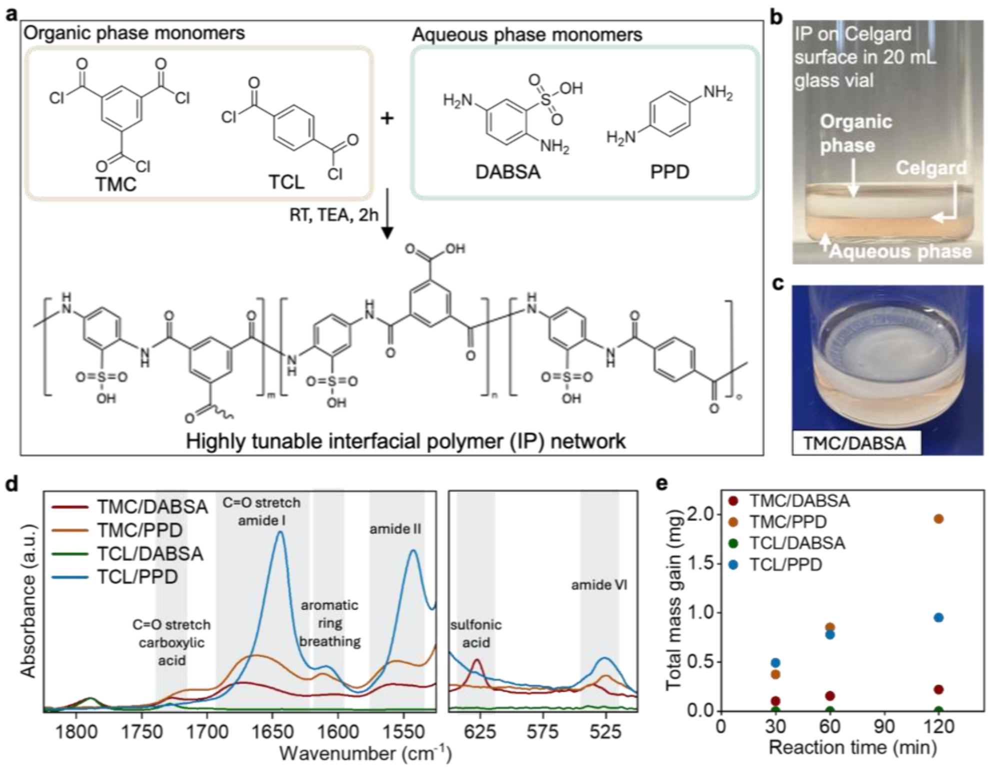

Figure 2: Fabrication of modified Celgard via a one-step interfacial polymerization reaction. a) Reaction scheme depicting selected monomers which can be tuned to modify the resulting polymer. b) Image of synthesis process with the Celgard resting at the interface of the aqueous and organic solutions in a glass vial. c) Image of the TMC/DABSA polymer formed on the Celgard after two hours. d) ATR-FTIR spectra of four interfacial polymers made from different combinations of TMC, TCL, DABSA and PPD. e) Cumulative mass gain of Celgard during interfacial polymer reaction between the four monomer combinations.

To understand how different monomer combinations affect film formation, we synthesized the following four thin film variations: TMC/DABSA, TMC/PPD, TCL/DABSA, and TCL/PPD. After conducting the reactions in the presence of Celgard and rinsing the resulting modified membranes first with ethanol followed by deionized water, we performed attenuated total reflectance Fourier Transform Infrared Spectroscopy (ATR-FTIR) to confirm successful polymer formation and adherence to the separator (**Figure 2d**). The ATR-FTIR spectra of the TMC/DABSA, TMC/PPD, and TCL/PPD films on Celgard all exhibit a peak at ~1650 cm^{-1} that can be attributed to C=O stretching of the newly formed amide group[31], confirming successful polymerization on Celgard with these monomer combinations. Among these, the peak intensity was highest for TCL/PPD, followed by TMC/PPD, then TMC/DABSA. Notably, the amide I peak was not present on Celgard after reaction with TCL/DABSA. The same trends were observed for the amide II and amide IV peaks.

Further observation revealed that the TMC/DABSA thin film formed only on the side of the separator facing the aqueous solution during the reaction, while the TMC/PPD film was present on both sides of the membrane (**Supplementary Figure 2**). ATR-FTIR results suggest PPD is significantly more mobile in the Celgard substrate and more reactive than DABSA, which was unable to form a film onto Celgard in the TCL/DABSA variation. The sulfonic acid group of DABSA is electron-withdrawing, thereby lowering the nucleophilicity of the diamine and limiting its reactivity. In the TCL/DABSA combination, we reason that the two active sites of TCL combined with the lower reactivity of DABSA do not allow sufficient polymerization to occur onto Celgard.

A distinct peak at ~628 cm^{-1} was observed exclusively in the TMC/DABSA membrane, which is attributed to C-S stretching[32] or SO_3 bending deformation[33] from the sulfonic acid groups introduced by DABSA. Although the peaks at 1140 cm^{-1} and 1080 cm^{-1} are more conventionally associated with sulfonic acid functionalities,[30] these signals overlap with absorption bands from the polypropylene/polyethylene Celgard substrate, making them difficult to resolve in the composite membrane. They can, however, be observed when TMC/DABSA is synthesized in absence of the Celgard in a "free-standing" version (**Supplementary Figure 3**), indicating the SO_3H groups remain after the polymerization reaction. The lack of sulfonic acid peak in the TCL/DABSA sample further confirms that the combination of the di-functional acyl chloride with less reactive sulfonated diamine does not form a thin film on Celgard.

Because the ATR-FTIR peak intensity suggests a large difference in kinetics of film formation, we performed a simple test to quantify how much mass was added to the Celgard over the duration of the polymerization reaction. We again synthesized the four variations of TMC or TCL and PPD or DABSA, and stopped the reaction at 30 minutes, 1 hour, and 2 hours to wash, dry, and weigh the Celgard (**Figure 2e**). The PPD-based films showed similar mass gains at 30 minutes and one hour; however, continued reaction in the TMC/PPD system resulted in a final mass increase of 1.957 mg after two hours, compared to 0.95 mg for TCL/PPD. Meanwhile, the TMC/DABSA film formation is slower, gradually rising to 0.22 mg after two hours. The TCL/DABSA film does not add any mass to the Celgard. These results demonstrate the greater reactivity of PPD over DABSA while suggesting that TCL's fewer acyl chloride reactive sites limit film formation compared to TMC. In addition to the higher reactivity of PPD over DABSA, the largest mass gain of TMC/PPD and the presence of the film on both sides of Celgard suggests PPD also has a higher diffusivity through the formed film that allows continuous reaction after film formation on the aqueous side. Notably, while TCL/PPD had the greatest intensity FTIR peaks from the thin film polyamide after interfacial polymerization, the lower mass relative to TMC/PPD suggests that TCL/PPD is more concentrated on the surface but is limited in growth. Thus, the higher FTIR intensity does not necessarily entail more polymer product was formed.

2.2 Tuning thin film crosslink density

For the Li-S battery, the goal is to achieve a moderately crosslinked sulfonated film that permits efficient Li-ion conduction through the separator while blocking LiPS diffusion via size exclusion and electrostatic repulsion. To accomplish this, the film crosslink density is tuned by adjusting the ratio of TMC and TCL, with the aim of balancing Li-ion transport and LiPS blocking. To explore this concept, thin films were fabricated on Celgard separators using the same one-step interfacial polymerization method, varying the TMC-to-TCL ratio in the organic phase while maintaining DABSA in the aqueous phase.

Three TMC-TCL ratios were explored: 20% TMC-80% TCL, 40% TMC-60% TCL, and 100%TMC-0%TCL. ATR-FTIR of the three ratios reveals that amide peak intensity increases with TMC fraction (**Figure 3a**). Some acyl chloride groups hydrolyze during the reaction, leading to the observed carboxylic acid peak at ~1723 cm^{-1}, yet the ratio of carboxylic acid:amide I is approximately the same for the three films. A distinct peak at 1790 cm^{-1}, corresponding to unreacted acyl chloride groups, appears most strongly in the 20% TMC film, decreases in the 40% TMC film, and is nearly absent in the 100% TMC film. These trends imply that higher TMC content, i.e. more acyl chloride functional groups, yields a greater degree of crosslinking with greater film formation,[34] in alignment with the increased mass gain observed over the two-hour reaction time for TMC-derived films compared to TCL-derived films (Section 2.1).

The 100% TMC film also has a higher intensity sulfonic acid peak at 637 cm^{-1}. These groups provide fixed negative charge which should contribute to electrostatic repulsion of LiPS transport across the thin film in the Li-S cell. Water contact angle measurements reveal that the 100% TMC film has the lowest contact angle of 47°, followed by 40% TMC at 91° and 20% TMC at 111°, resembling the bare Celgard (**Figure 3b**). Combined with the ATR-FTIR observations, the enhanced hydrophilicity of the 100% TMC film suggests that this chemistry achieves the highest amount of sulfonated thin film formation on the surface of the modified Celgard, which should enhance LiPS repulsion.

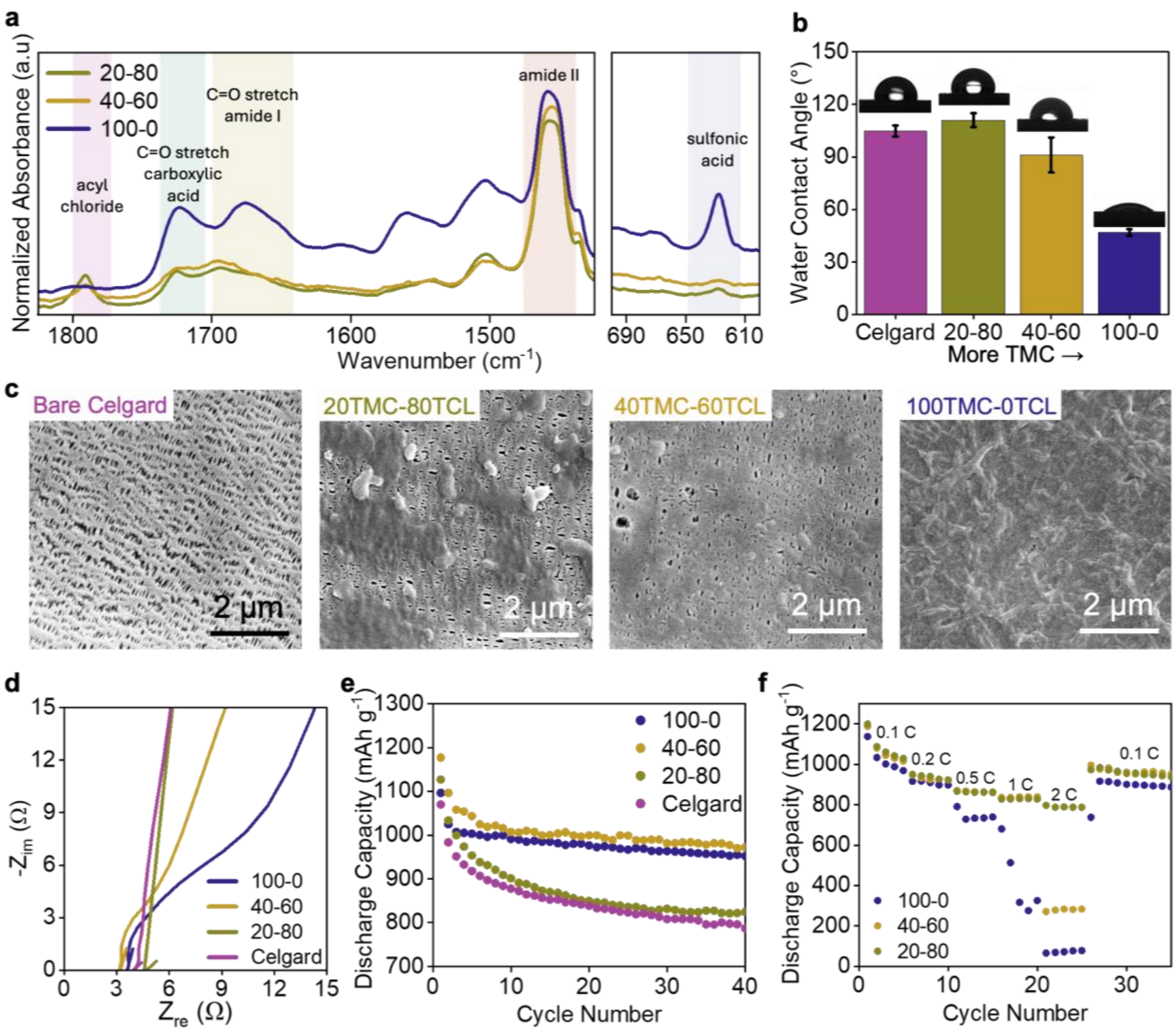

Figure 3: Tuning TMC/TCL organic phase ratio of polymer formed on Celgard separator. In the legends, the first number corresponds to % TMC and the second number corresponds to % TCL used in the organic phase during polymerization. a) ATR-FTIR spectra of polymers formed varying the ratio of organic phase monomers. b) Water contact angle measurements on Celgard and the modified separators. c) SEM images of bare and modified Celgard with different ratios of organic phase monomers. d) Impedance spectra of stainless-steel blocking electrode coin cells, varying the separator. e) Discharge capacity of Li-S cells at 0.2 C. f) Rate performance tests of Li-S cells from 0.1 C to 2 C.

Scanning electron microscopy (SEM) was employed to examine the effect of varying the organic monomer ratio on film morphologies (**Figure 3c**). Compared to bare Celgard, 20% TMC has uncoated regions where the underlying Celgard pores can be observed. Other regions, however, are more densely covered, highlighting the significant film inhomogeneity at 20% TMC. When TMC content is increased to 40%, the film becomes more uniform with smaller macro pores, while 100% TMC leads to the most uniform film with few observable pores from the underlying substrate at this scale. Pore size analysis of the SEM results emphasizes that the 100% TMC modification yields the fewest surface pores (~ 2.5 pores μm^{-2}). Reducing the TMC:TCL ratio increases the number of pores closer to the count of bare Celgard (**Supplementary Figure 4**). These observations suggest that higher TMC content films leads to denser crosslinking and substrate pore coverage, while TCL dominated films retain larger macropores. The 20% TMC-80% TCL film likely has insufficient crosslinks that result in inhomogeneity and overall poor coverage. When paired with the less reactive DABSA diamine monomer, higher TMC content is needed for good film integrity.

Electrochemical impedance spectroscopy (EIS) was used to investigate the effect of varying TMC/TCL ratios on ionic conductivity (**Figure 3d**). Coin cells with stainless steel blocking electrodes and conventional ether electrolyte were assembled for EIS. The x-intercept, indicative of the bulk cell resistance, R_b, is inversely proportional to the ionic conductivity through the relation $\sigma = L/(R_b \times A)$, where σ is ionic conductivity, L is thickness of the ion conductor, and A is the cross-sectional area. The 40% film yields the lowest value x-intercept in the Nyquist plot, implying the highest ionic conductivity. L and A are assumed approximately the same for all membranes because the DABSA-based thin films add <1% thickness to the 25 μm Celgard. (**Supplementary Figure 5**). The conductivity improvement over bare Celgard may be from the presence of sulfonic acid groups which can improve electrolyte wetting of the separator.[35] The 100% TMC film, though shown to be more hydrophilic, may suffer from coverage of the Celgard substrate pores observed in the SEM, and has the second lowest bulk resistance. R_b of the 20% TMC film is just above that of bare Celgard, possibly due to the inhomogeneous regions of dense film formation. Notably, however, an additional semi-circle is observed for the 40% and 100% TMC films. This extra resistance may signify a contact or interfacial resistance imparted by the higher TMC films, which could undermine their lower bulk resistances.

2.3 Integrating the modified separators into Li-S batteries

The effectiveness of the modified separators in Li-S batteries was evaluated by assembling cells with a lithium anode, sulfur cathode, and the respective Celgard separator: bare, and with the 20%, 40%, or 100% TMC film (**Figure 3e**). The separator containing 20% TMC exhibited minimal improvement in capacity retention compared to the bare Celgard. The first discharge capacity of bare Celgard is 1069.6 mAh g^{-1}, which drops to 787.2 mAh g^{-1} by cycle 40. The 20% TMC-80% TCL separator enables a larger initial capacity of 1127 mAh g^{-1}, but the capacity drops to 824.9 mAh g^{-1} by cycle 40. When the 40% TMC and 100% TMC films on Celgard are employed, the capacity retention is significantly improved. The initial capacities of the 40% and 100% TMC cells are 1176.7 mAh g^{-1} and 1096.4 mAh g^{-1}, still reaching 972.3 mAh g^{-1} and 952 mAh g^{-1} respectively by cycle 40. Notably, higher TMC content above 40% does not lead to further capacity retention, and the benefit of the DABSA-based film appears to be maximized with the 40% TMC-60% TCL ratio under these cycling conditions.

Building upon the capacity retention results, rate performance was evaluated to further investigate the influence of the TMC-TCL thin films on sulfur cathode reaction kinetics. Cells were cycled at a progressively increasing rate from 0.1 C up to 2 C (**Figure 3f**). Despite the enhanced capacity retention at 0.2 C, the cell with the 100% TMC-0% TCL modified separator becomes unstable at 1 C and hardly delivers any capacity at 2 C. The 40% TMC-60% TCL can perform at 1 C, delivering up to 838.2 mAh g^{-1}, while the 20% TMC-80%TCL cell delivers a slightly lower capacity of up to 829.4 mAh g^{-1} at 1 C. However, when the rate is increased to 2 C, the cell with the 40% TMC separator can reach only 283 mAh $g^{-1.}$ The 20% TMC cell, on the other hand, maintains significant capacity of up to 795.9 mAh g^{-1} at 2 C. These results indicate that although higher TMC content enhances capacity retention at lower rates, films containing ≥ 40% TMC impose kinetic limitations that hinder performance at elevated rates. This poor rate performance is likely a result of the added resistance observed in the Nyquist plots discussed above.

2.4 Improving film coverage via PPD addition

Despite its inhomogeneity, the 20% TMC-80% TCL film is the only modified cell that can cycle with good capacity from 0.1 C up to 2C. This behavior identifies the 20% TMC film as a promising candidate for further development, provided that its film integrity can be enhanced. As previously demonstrated, the DABSA monomer exhibits significantly lower reactivity compared to the non-sulfonated PPD monomer, which may contribute to the observed structural issues. To address this, a small amount of PPD (0.25 wt% relative to DABSA) was added to the aqueous DABSA solution for film preparation. The inclusion of PPD is intended to improve the film integrity while maintaining the rate performance of the 20% TMC-80% TCL framework. A low concentration of PPD was chosen, as higher PPD content would for a denser film and cause detrimental pore closure. In the following discussion, the DABSA-based film is referred to as "20% TMC-80% TCL", while the film with DABSA and PPD is distinguished as "20% TMC-80% TCL + PPD".

X-ray photoelectron spectroscopy (XPS) was conducted on the standalone modified Celgard separators to evaluate the influence of PPD on the film formation. Since the interfacial polymer is the only nitrogen-containing component in the separator, the N/C atomic ratio serves as an indicator of film formation at various depths (**Figure 4a**). The addition of PPD results in increased nitrogen content at the separator surface, which gradually decreases with increasing sputter depth. In contrast, the DABSA-only separator exhibits lower nitrogen content, suggesting reduced film formation. To assess whether PPD displaces DABSA in the polymerization processes, the S/C atomic ratio was also examined. The sulfur signal, associated with the sulfonated DABSA monomer, remains consistent across the depth profile in the presence of PPD and decreases as the analysis proceeds into the Celgard substrate. This result indicates that DABSA incorporation is retained and not significantly displaced by PPD, thereby preserving the electrostatic polysulfide-blocking functionality (**Supplementary Figure 6**).

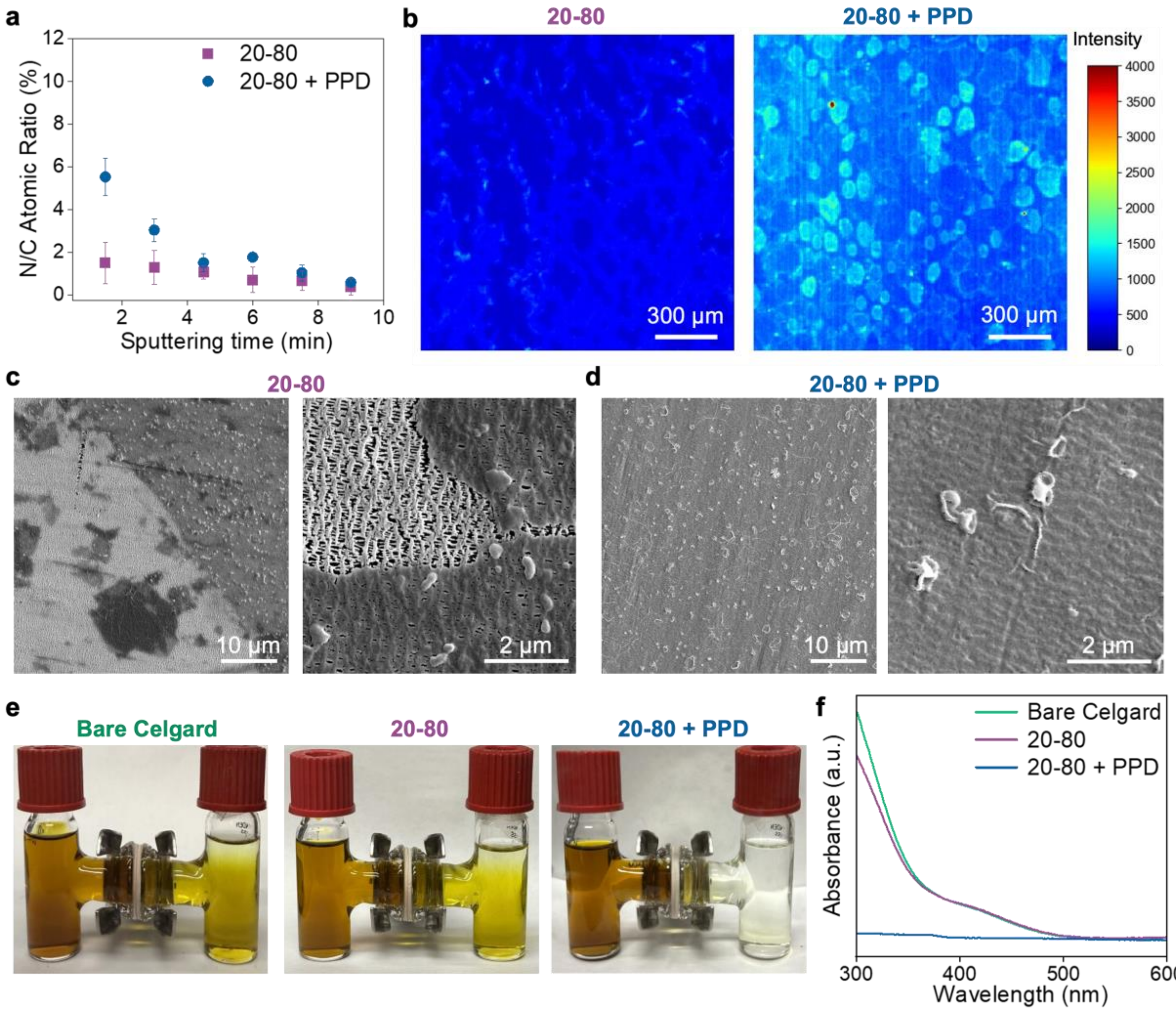

Figure 4: Characterization of Celgard modified by 20% TMC-80% TCL (in figure, abbreviated as "20-80") film with and without PPD added to DABSA in aqueous phase. a) N/C atomic ratios from XPS. b) Sulfur XRF maps at an X-ray energy of 2481.2 eV. SEM images of 20% TMC-80% TCL films with DABSA only (c) and with PPD added to aqueous phase of interfacial polymerization (d). e) H-cell experiments to observe polysulfide diffusion after four hours across bare Celgard, Celgard with the 20% TMC-80% TCL film, and Celgard with the 20% TMC- 80% TCL + PPD film. f) UV-Vis of the right side solution after allowing four hours of polysulfide diffusion.

X-ray fluorescence (XRF) mapping at the absorption peak of the S K-edge XANES 2481.2 eV) in the two films provides additional confirmation that PPD enhances DABSA-containing film coverage (**Figure 4b**). The sulfur K-edge XANES spectra further show that there are not noticeable changes in the chemical state of sulfur before and after interfacial polymerization (**Supplementary Figure 7**). The average S-intensity observed on the 20%TMC-80%TCL + PPD film is approximately 3 times higher than the highest intensity sulfur regions in the 20-80 film. Additionally, while the 20%TMC-80%TCL film has large regions without sulfur, the 20%TMC-80%TCL + PPD film is consistently covered by S-containing film. Irregular ovular regions with elevated sulfur intensity are observed in the 20%TMC-80%TCL + PPD film, potentially resulting from local variations in film thickness on the Celgard substrate (**Supplementary Figure 8 and 9**). Despite this, the XAS result confirms that the incorporation of PPD improves sulfonated polyamide film coverage over the whole area of Celgard measured, while using DABSA alone in the aqueous phase causes large regions with no sulfur (i.e. no thin film) present.

This observation aligns with our SEM images of these films: SEM of the 20% TMC-80% TCL separator with only DABSA in the aqueous solution again reveals the inhomogeneity of film coverage (**Figure 4c**). However, when PPD is added, the film becomes significantly more homogenous with strong coverage, and few underlying Celgard substrate pores can be observed at this scale (**Figure 4d**). Thus, PPD significantly improves film coverage at the low TMC content.

H-cell experiments were employed to visualize the impact of the modified membranes on polysulfide shuttle behavior (**Figure 4e**). With bare Celgard and 20% TMC-80% TCL, there is significant diffusion of polysulfide through the separator after four hours. However, in the 20% TMC-80% TCL + PPD, little polysulfide diffusion is observed over the same time period. This result is confirmed by UV-Vis of the right-side of the H-cell after four hours (**Figure 4f**). With PPD, lower absorbance is observed in the region in which the dark-colored polysulfide absorbs light. Meanwhile, the 20% TMC-80% TCL separator without PPD yields a solution with just a slightly lower absorbance in this region than the bare Celgard.

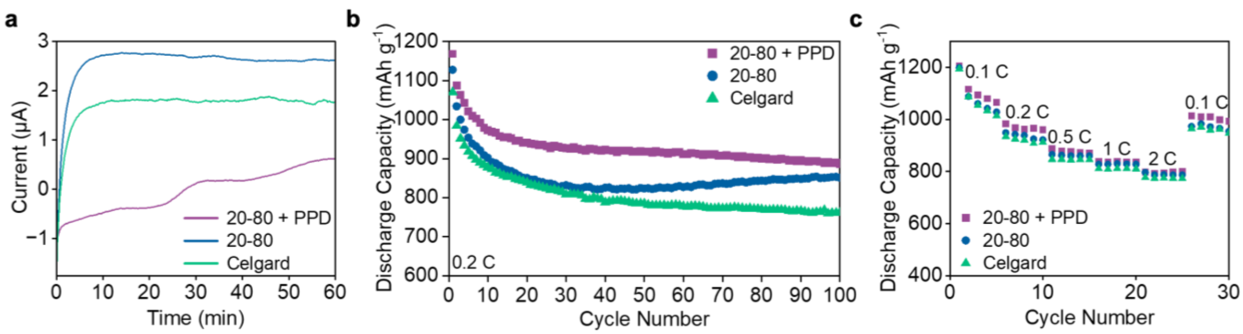

Figure 5: Electrochemical performance of Li-S coin cells with 20% TMC-80% TCL (in figure, abbreviated as “20-80”) with and without PPD, and bare Celgard separators. a) Shuttle current measurement over one hour at 2.3 V. b) Cycling performance at 0.2 C-rate. c) Rate performance test from 0.1 C to 2 C.

Shuttle current measurements can be used to quantitively measure the shuttle effect in coin cells.[36] Following a three-cycle activation at 0.05C, the cells were paused at 2.3V, at which the concentration of LiPS is expected to be high. The cells were then held at OCV, and the current required to maintain this voltage was measured. A more positive current is indicative of more polysulfide shuttling. The bare Celgard and 20%TMC-80%TCL cells display a shuttle current of about 1.8 and 2.6 μA respectively. This current is well above that of the 20%TMC-80%TCL + PPD which begins at a negative value (likely from disproportionation of sulfur species[36] and slowly reaches 0.6 μA by the end of the test. As supported by the H-cell measurement, the addition of PPD effectively mitigates polysulfide shuttling.

Although the 20% TMC- 80% TCL + DABSA separator without PPD did not outperform higher TMC content films in terms of capacity retention, the improved film integrity achieved with the DABSA/PPD combination was further evaluated (**Figure 5a**). The addition of PPD resulted in a separator delivering an initial discharge capacity of 1167 mAh g^{-1} and 921.8 mAh g^{-1} by cycle 40 (**Figure 5b**). Conversely, as reported above in Figure 3e and shown again here, 20% TMC-80% TCL without PPD delivers a lower 1127 mAh g^{-1} on the first discharge which falls to 824.9 mAh g^{-1} after 40 cycles. These results indicate that adding PPD into the interfacial polymerization improves the capacity retention for the lower TMC content film.

Significantly, the addition of low PPD does not negatively affect the rate performance up to 2 C (**Figure 5c**). 20%TMC-80%TCL + PPD can deliver up to 800.7 mAh g^{-1} at 2C, even slightly higher than the 795.9 mAh g^{-1} and 776.6 mAh g^{-1} at 2C for 20% TMC-80% TCL without PPD and the bare Celgard respectively. Further, adding PPD enables the highest discharge capacity (1014.1 mAh g^{-1}) upon returning to 0.1C at cycle 26.

3 Conclusion

In summary, a one-step, scalable method has been demonstrated for fabricating highly tunable polymer networks directly onto commercial Celgard separators. The DABSA aqueous-phase monomer provides effective polysulfide rejection, while a low content of tri-functionalized TMC crosslinker mitigates the kinetic limitations observed in highly crosslinked films. Yet, to achieve film homogeneity and integrity at this low TMC content, we add the more reactive PPD monomer while still including DABSA in the formed polymer film. The resulting 20% TMC- 80% TCL PPD film is able to maintain 921.8 mAh g^{-1} at 0.2 C-rate after 40 cycles due to its demonstrated ability to block polysulfide shuttle. Despite its dense coverage of the Celgard surface pores as revealed by SEM, the 20% TMC-80% TCL + PPD film can also reach a high capacity of over 800 mAh g^{-1} at 2 C, highlighting an effective strategy to block the shuttle effect while minimizing kinetic limitations. Future work could investigate interfacial polymerization using different sulfonated monomers or the incorporation of conductive and/or catalytic materials directly into the film to further enhance the positive effect on Li-S battery performance. We believe this is a highly adaptable and accessible method to tune the properties of commercial separators and can also be applied to other chemistries and membrane-based applications.

Acknowledgement:
Part of this work was performed at the Stanford Nano Shared Facilities (SNSF) RRID:SCR_023230, supported by the National Science Foundation under award ECCS-2026822. Use of the Stanford Synchrotron Radiation Lightsource at SLAC National Accelerator Laboratory is supported by the U.S. Department of Energy, Office of Science, Office of Basic Energy Sciences under Contract No. DE-AC02-76SF00515. L.C.G. acknowledges support from the National Science Foundation Graduate Research Fellowship under Grant 2146755. Y. C. acknowledges supports from the Japan Society for the Promotion of Science (JSPS) overseas research fellowship and the Stanford Energy Postdoctoral Fellowship and the Precourt Institute for Energy. Y.-K. Tzeng and Y. Cui acknowledges the support from U.S. Department of Energy of the Battery500 Consortium and BMR programs. K.A. and W.A.T acknowledge support from the Stanford Department of Chemical Engineering, the Precourt Energy Institute and StorageX Initiative, and the Stanford Graduate Fellowship.

Author Contribution:
L.C.G., K.A., and Y.-K.T. conceived the project and designed the experiments. Y.C. performed XAS mapping measurement and data analysis. H.A. assisted with sample preparation and performed sputtering. L.C.G. and K.A. wrote the manuscript. Y.-K. T., W.T., and Y.C. supervised the project. All authors discussed the results and commented on the manuscript.

References:

(1) Cano, Z. P.; Banham, D.; Ye, S.; Hintennach, A.; Lu, J.; Fowler, M.; Chen, Z. Batteries and Fuel Cells for Emerging Electric Vehicle Markets. *Nat Energy* **2018**, *3* (4), 279–289. https://doi.org/10.1038/s41560-018-0108-1.

(2) Sun, J.; Wang, T.; Gao, Y.; Pan, Z.; Hu, R.; Wang, J. Will LITHIUM-SULFUR Batteries Be the next BEYOND-LITHIUM Ion Batteries and Even Much Better? *InfoMat* **2022**, *4* (9), e12359. https://doi.org/10.1002/inf2.12359.

(3) Zhou, G.; Chen, H.; Cui, Y. Formulating Energy Density for Designing Practical Lithium–Sulfur Batteries. *Nat Energy* **2022**, *7* (4), 312–319. https://doi.org/10.1038/s41560-022-01001-0.

(4) Manthiram, A.; Chung, S.-H.; Zu, C. Lithium-Sulfur Batteries: Progress and Prospects. *Adv. Mater.* **2015**, *27* (12), 1980–2006. https://doi.org/10.1002/adma.201405115.

(5) Capkova, D.; Knap, V.; Fedorkova, A. S.; Stroe, D.-I. Analysis of 3.4 Ah Lithium-Sulfur Pouch Cells by Electrochemical Impedance Spectroscopy. *Journal of Energy Chemistry* **2022**, *72*, 318–325. https://doi.org/10.1016/j.jechem.2022.05.026.

(6) Li, S.; Jin, B.; Zhai, X.; Li, H.; Jiang, Q. Review of Carbon Materials for Lithium-Sulfur Batteries. *ChemistrySelect* **2018**, *3* (8), 2245–2260. https://doi.org/10.1002/slct.201703112.

(7) Li, X.; Sun, X. Interface Design and Development of Coating Materials in Lithium–Sulfur Batteries. *Adv Funct Materials* **2018**, *28* (30), 1801323. https://doi.org/10.1002/adfm.201801323.

(8) Liu, D.; Zhang, C.; Zhou, G.; Lv, W.; Ling, G.; Zhi, L.; Yang, Q. Catalytic Effects in Lithium–Sulfur Batteries: Promoted Sulfur Transformation and Reduced Shuttle Effect. *Advanced Science* **2018**, *5* (1), 1700270. https://doi.org/10.1002/advs.201700270.

(9) Wei Seh, Z.; Li, W.; Cha, J. J.; Zheng, G.; Yang, Y.; McDowell, M. T.; Hsu, P.-C.; Cui, Y. Sulphur–TiO2 Yolk–Shell Nanoarchitecture with Internal Void Space for Long-Cycle Lithium–Sulphur Batteries. *Nat Commun* **2013**, *4* (1), 1331. https://doi.org/10.1038/ncomms2327.

(10) Zhou, W.; Yu, Y.; Chen, H.; DiSalvo, F. J.; Abruña, H. D. Yolk–Shell Structure of Polyaniline-Coated Sulfur for Lithium–Sulfur Batteries. *J. Am. Chem. Soc.* **2013**, *135* (44), 16736–16743. https://doi.org/10.1021/ja409508q.

(11) Yang, Y.; Zheng, G.; Cui, Y. Nanostructured Sulfur Cathodes. *Chem. Soc. Rev.* **2013**, *42* (7), 3018. https://doi.org/10.1039/c2cs35256g.

(12) Li, W.; Yao, H.; Yan, K.; Zheng, G.; Liang, Z.; Chiang, Y.-M.; Cui, Y. The Synergetic Effect of Lithium Polysulfide and Lithium Nitrate to Prevent Lithium Dendrite Growth. *Nat Commun* **2015**, *6* (1), 7436. https://doi.org/10.1038/ncomms8436.

(13) Zhang, L.; Ling, M.; Feng, J.; Mai, L.; Liu, G.; Guo, J. The Synergetic Interaction between LiNO3 and Lithium Polysulfides for Suppressing Shuttle Effect of Lithium-Sulfur Batteries. *Energy Storage Materials* **2018**, *11*, 24–29. https://doi.org/10.1016/j.ensm.2017.09.001.

(14) Liu, Y.; Elias, Y.; Meng, J.; Aurbach, D.; Zou, R.; Xia, D.; Pang, Q. Electrolyte Solutions Design for Lithium-Sulfur Batteries. *Joule* **2021**, *5* (9), 2323–2364. https://doi.org/10.1016/j.joule.2021.06.009.

(15) Deng, N.; Kang, W.; Liu, Y.; Ju, J.; Wu, D.; Li, L.; Hassan, B. S.; Cheng, B. A Review on Separators for Lithium Sulfur Battery: Progress and Prospects. *Journal of Power Sources* **2016**, *331*, 132–155. https://doi.org/10.1016/j.jpowsour.2016.09.044.

(16) Parikh, D.; Christensen, T.; Hsieh, C.-T.; Li, J. Elucidation of Separator Effect on Energy Density of Li-Ion Batteries. *J. Electrochem. Soc.* **2019**, *166* (14), A3377–A3383. https://doi.org/10.1149/2.0571914jes.

(17) Cheng, P.; Guo, P.; Sun, K.; Zhao, Y.; Liu, D.; He, D. CeO2 Decorated Graphene as Separator Modification Material for Capture and Boost Conversion of Polysulfide in Lithium-Sulfur Batteries. *Journal of Membrane Science* **2021**, *619*, 118780. https://doi.org/10.1016/j.memsci.2020.118780.

(18) Chung, S.; Manthiram, A. Bifunctional Separator with a Light-Weight Carbon-Coating for Dynamically and Statically Stable Lithium-Sulfur Batteries. *Adv Funct Materials* **2014**, *24* (33), 5299–5306. https://doi.org/10.1002/adfm.201400845.

(19) Yang, D.; Zhi, R.; Ruan, D.; Yan, W.; Zhu, Y.; Chen, Y.; Fu, L.; Holze, R.; Zhang, Y.; Wu, Y.; Wang, X. A Multifunctional Separator for High-Performance Lithium-Sulfur Batteries. *Electrochimica Acta* **2020**, *334*, 135486. https://doi.org/10.1016/j.electacta.2019.135486.
(20) Bai, S.; Liu, X.; Zhu, K.; Wu, S.; Zhou, H. Metal–Organic Framework-Based Separator for Lithium–Sulfur Batteries. *Nat Energy* **2016**, *1* (7), 16094. https://doi.org/10.1038/nenergy.2016.94.
(21) Zhao, J.; Yan, G.; Zhang, X.; Feng, Y.; Li, N.; Shi, J.; Qu, X. In Situ Interfacial Polymerization of Lithiophilic COF@PP and POP@PP Separators with Lower Shuttle Effect and Higher Ion Transport for High-Performance Li–S Batteries. *Chemical Engineering Journal* **2022**, *442*, 136352. https://doi.org/10.1016/j.cej.2022.136352.
(22) Lee, J. H.; Yeon, J. S.; Kim, J.; Park, J. H.; Yoo, S. S.; Hong, S.; Kim, M.; Park, M. J.; Park, H. S.; Yoo, P. J. Accelerated Li-Ion Transport through a Zwitterion-Anchored Separator for High-Performance Li–S Batteries. *J. Mater. Chem. A* **2021**, *9* (45), 25463–25473. https://doi.org/10.1039/D1TA08422D.
(23) Huang, J.-Q.; Zhang, Q.; Peng, H.-J.; Liu, X.-Y.; Qian, W.-Z.; Wei, F. Ionic Shield for Polysulfides towards Highly-Stable Lithium–Sulfur Batteries. *Energy Environ. Sci.* **2014**, *7* (1), 347–353. https://doi.org/10.1039/C3EE42223B.
(24) Song, S.; Shi, L.; Lu, S.; Pang, Y.; Wang, Y.; Zhu, M.; Ding, D.; Ding, S. A New Polysulfide Blocker - Poly(Acrylic Acid) Modified Separator for Improved Performance of Lithium-Sulfur Battery. *Journal of Membrane Science* **2018**, *563*, 277–283. https://doi.org/10.1016/j.memsci.2018.05.050.
(25) Kim, S. H.; Yeon, J. S.; Kim, R.; Choi, K. M.; Park, H. S. A Functional Separator Coated with Sulfonated Metal–Organic Framework/Nafion Hybrids for Li–S Batteries. *J. Mater. Chem. A* **2018**, *6* (48), 24971–24978. https://doi.org/10.1039/C8TA08843H.
(26) Dezhi Yang; Xiong, X.; Zhu, Y.; Chen, Y.; Fu, L.; Zhang, Y.; Wu, Y. Modifications of Separators for Li–S Batteries with Improved Electrochemical Performance. *Russ J Electrochem* **2020**, *56* (4), 365–377. https://doi.org/10.1134/S1023193520050110.
(27) Li, C.; Liu, R.; Xiao, Y.; Cao, F.; Zhang, H. Recent Progress of Separators in Lithium-Sulfur Batteries. *Energy Storage Materials* **2021**, *40*, 439–460. https://doi.org/10.1016/j.ensm.2021.05.034.
(28) Xu, X.; Yang, Y.; Liu, T.; Chu, B. Cost-Effective Polymer-Based Membranes for Drinking Water Purification. *Giant* **2022**, *10*, 100099. https://doi.org/10.1016/j.giant.2022.100099.
(29) Ismail, A. F.; Padaki, M.; Hilal, N.; Matsuura, T.; Lau, W. J. Thin Film Composite Membrane — Recent Development and Future Potential. *Desalination* **2015**, *356*, 140–148. https://doi.org/10.1016/j.desal.2014.10.042.
(30) Ruiz-Torres, C. A.; Zhu, J.; Riet, J. A.; Sarker, N. R.; Abu-Obaid, S.; Yuan, K. D.; De Lannoy, C.-F.; Werber, J. R. Ultra-Thin Cation Exchange Membranes: Sulfonated Polyamide Thin-Film Composite Membranes with High Charge Density. *Chem. Mater.* **2024**, *36* (22), 11217–11226. https://doi.org/10.1021/acs.chemmater.4c02270.
(31) Tang, C.; Kwon, Y.; Leckie, J. Probing the Nano- and Micro-Scales of Reverse Osmosis Membranes—A Comprehensive Characterization of Physiochemical Properties of Uncoated and Coated Membranes by XPS, TEM, ATR-FTIR, and Streaming Potential Measurements. *Journal of Membrane Science* **2007**, *287* (1), 146–156. https://doi.org/10.1016/j.memsci.2006.10.038.
(32) Laporta, M.; Pegoraro, M.; Zanderighi, L. Perfluorosulfonated Membrane (Nafion): FT-IR Study of the State of Water with Increasing Humidity. *Phys. Chem. Chem. Phys.* **1999**, *1* (19), 4619–4628. https://doi.org/10.1039/a904460d.
(33) Aydin, M. Comparative Study of the Structural and Vibroelectronic Properties of Porphyrin and Its Derivatives. *Molecules* **2014**, *19* (12), 20988–21021. https://doi.org/10.3390/molecules191220988.
(34) Liu, Y.; Tian, M.; Zhang, W.; Hu, B.; Deng, H. Enhancing Monovalent Selectivity of Cation Exchange Membranes by Electric Field-Assisted Interfacial Polymerization. *Journal of Membrane Science* **2025**, *733*, 124291. https://doi.org/10.1016/j.memsci.2025.124291.

(35) Ding, H.; Ge, J.; Zhang, T.; He, C.; Zhang, H.; Mohamad Ali, B.; Wang, J. Thermally Stable Poly-Aromatic Solid Electrolyte Coated Polyethylene Membrane as High-Performance Lithium-Ion Battery Separator. *Journal of Power Sources* **2024**, *602*, 234355. https://doi.org/10.1016/j.jpowsour.2024.234355.
(36) Moy, D.; Manivannan, A.; Narayanan, S. R. Direct Measurement of Polysulfide Shuttle Current: A Window into Understanding the Performance of Lithium-Sulfur Cells. *J. Electrochem. Soc.* **2015**, *162* (1), A1–A7. https://doi.org/10.1149/2.0181501jes.